Postsynaptic activity reverses the sign of the acetylcholine-induced long-term plasticity of $GABA_A$ inhibition

Soledad Domínguez[a], David Fernández de Sevilla[a,b], and Washington Buño[a,1]

[a]Instituto Cajal, Consejo Superior de Investigaciones Científicas, 28002 Madrid, Spain; and [b]Departamento de Anatomía, Histología y Neurociencia, Facultad de Medicina, Universidad Autónoma de Madrid, 28029 Madrid, Spain

Edited by Roberto Malinow, University of California, San Diego, La Jolla, CA, and approved May 20, 2014 (received for review November 20, 2013)

Acetylcholine (ACh) regulates forms of plasticity that control cognitive functions but the underlying mechanisms remain largely unknown. ACh controls the intrinsic excitability, as well as the synaptic excitation and inhibition of CA1 hippocampal pyramidal cells (PCs), cells known to participate in circuits involved in cognition and spatial navigation. However, how ACh regulates inhibition in function of postsynaptic activity has not been well studied. Here we show that in rat PCs, a brief pulse of ACh or a brief stimulation of cholinergic septal fibers combined with repeated depolarization induces strong long-term enhancement of $GABA_A$ inhibition ($GABA_A$-LTP). Indeed, this enhanced inhibition is due to the increased activation of $\alpha_5\beta\gamma_2$ subunit-containing $GABA_A$ receptors by the GABA released. $GABA_A$-LTP requires the activation of M1-muscarinic receptors and an increase in cytosolic Ca^{2+}. In the absence of PC depolarization ACh triggered a presynaptic depolarization-induced suppression of inhibition (DSI), revealing that postsynaptic activity gates the effects of ACh from presynaptic DSI to postsynaptic LTP. These results provide key insights into mechanisms potentially linked with cognitive functions, spatial navigation, and the homeostatic control of abnormal hyperexcitable states.

endocannabinoids | intracellular Ca^{2+} | LTP of inhibition | outward rectification

Long-term potentiation (LTP) at excitatory synapses is thought to be the cellular substrate of learning of the brain. Less is known about LTP at inhibitory synapses, a vital process given that inhibition regulates network behavior and LTP at excitatory synapses (1–3). Cholinergic activity can influence intrinsic excitability, as well as both excitatory (4, 5) and inhibitory synaptic plasticity (6, 7). However, less is known about the postsynaptic cholinergic-mediated control of synaptic inhibition and specifically of its regulation by postsynaptic activity. The CA1 region of the hippocampus receives a significant cholinergic projection from the medial septal nuclei (8). These act primarily through acetylcholine (ACh) muscarinic receptors (mAChRs) on CA1 pyramidal cells (PCs) (9), as well as through mAChRs and nicotinic cholinergic receptors (nAChRs) on interneurons (10). In addition, the retrograde modulation of γ-aminobutyric acid (GABA)-mediated inhibition by endocannabinoids (eCBs) (11) and its regulation by ACh and postsynaptic activity have been analyzed (12).

We analyzed the modifications induced in PCs in the CA1 of rat hippocampal slices by repeated postsynaptic depolarization, applied in combination with a single brief ACh pulse delivered to the apical dendritic shaft. The postsynaptic depolarization reproduced either the rhythmic bursting that typifies the hippocampal theta rhythm [i.e., theta burst stimulation (TBS)] or that of prolonged repeated depolarization. Indeed, these protocols induced a robust long-term enhancement of inhibition because of the increased activation of $\alpha_5\beta\gamma_2$ subunit-containing $GABA_A$ receptors ($GABA_A$Rs) by the released GABA, with no involvement of $GABA_B$Rs. We termed this long-term enhancement of inhibition $GABA_A$-LTP. $GABA_A$-LTP was also evoked by a physiological relevant stimulation of cholinergic septal fibers of the oriens/alveus (*O/A*), combined with repeated depolarization or TBS stimulation. This $GABA_A$-LTP required activation of the M1 subtype mAChRs (M1-mAChRs) and an increased cytosolic Ca^{2+}. In the absence of postsynaptic depolarization, ACh generated a type 1 eCB receptor (CB_1R)-dependent depolarization-induced suppression of inhibition (DSI) (13), indicating that the effects of ACh on synaptic inhibition depend on the active or quiescent state of the postsynaptic PC. Therefore, ACh triggers a state-dependent gating that transfers the dominant effects of postsynaptic activity from presynaptic DSI to postsynaptic LTP. Such a relocation may be essential to regulate the network activity that may be linked to the information-processing capacity of the system in terms of spatial and cognitive functions (14) and of the homeostatic control of abnormal hyperexcitable states.

Results

The ACh Pulse and Repeated Depolarization Induce the $GABA_A$-LTP. Under voltage-clamp conditions with a 10-mM Cl^- intracellular solution and a calculated chloride equilibrium potential (ECl^-) of −64.7 mV, *stratum radiatum* (SR) stimulation provoked brief negative-going control inhibitory postsynaptic currents (IPSCs) at −75 mV that had mean peak amplitudes of −16.6 ± 5.14 pA. All measurements were made on the first (R1) IPSC of the pair, except when indicated otherwise. We stimulated the PC with the intracellular TBS protocol used throughout the experiment (Fig. 1 *B* and *C*) and applied the ACh pulse (Fig. 1*D*, open arrow). ACh induced a gradual enhancement of the IPSC peak amplitude (i.e., the $GABA_A$-LTP), which reached a steady state of 242 ± 18% of the controls ($P < 0.001$; $N = 8$) in ∼20 min and lasted at least 1 h (Fig. 1*D*, solid circles), and no important

Significance

Cholinergic activity regulates excitability and plasticity in neuronal circuits through the activation of muscarinic and nicotinic receptors. Here we demonstrate that muscarinic receptors can depress or enhance synaptic inhibition in the hippocampal CA1 region, depending on the quiescent or active state of the postsynaptic target CA1 pyramidal neuron, the main hippocampal CA1 output. These effects regulate inhibition from a presynaptic to a postsynaptic site, a relocation that could be essential to control activity associated with cognitive functions and the homeostatic regulation of abnormal hyperexcitability.

Author contributions: D.F.d.S. and W.B. designed research; S.D. performed research; S.D., D.F.d.S., and W.B. contributed new reagents/analytic tools; S.D., D.F.d.S., and W.B. analyzed data; and S.D., D.F.d.S., and W.B. wrote the paper.

The authors declare no conflict of interest.

This article is a PNAS Direct Submission.

[1]To whom correspondence should be addressed. E-mail: wbuno@cajal.csic.es.

This article contains supporting information online at www.pnas.org/lookup/suppl/doi:10.1073/pnas.1321777111/-/DCSupplemental.

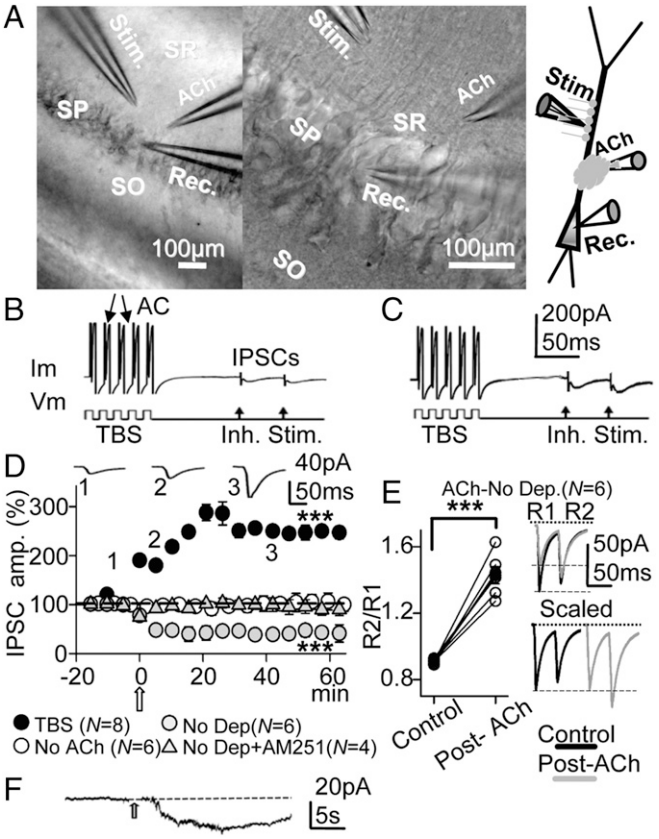

Fig. 1. The effects of ACh depend on the quiescent or active state of the CA1 pyramidal neuron. (*A*) (*Left* and *Center*) DIC photomicrographs showing the *stratum pyramidale*, *oriens*, and *radiatum* (SP, SO and SR, respectively) in the slice and the sites of the recording (Rec.), stimulation (Stim.), and ACh microiontophoresis pipettes. (*Right*) Schematic diagram of the experimental setup. (*B*) Example of pre-ACh control response evoked under voltage clamp by the TBS protocol and paired-pulse stimulation, showing action currents (AC) and IPSC pair. (*C*) Same cell as *B*, but recorded during the $GABA_A$-LTP 30 min post-ACh. (*D*) (solid circles) Plot of the average peak IPSC amplitude (percentage of the first IPSC in controls) vs. time recorded with 10-mM Cl^- intracellular solution and showing the $GABA_A$-LTP. Each circle represents the average peak amplitude of the IPSCs recorded over 5 min and the open arrow indicates the ACh pulse, as in Figs. 1–7 and Figs. S1–S3. The upper recordings are IPSC averages ($n = 10$) from a representative experiment at time points 1, 2 and 3. (Open circles) Same as solid circles, but showing that the TBS did not modify IPSCs in the absence of the ACh pulse. (Shaded circles) Same as solid circles, but showing that ACh induced DSI at −75 mV in the absence of TBS. (Shaded triangles) Same as shaded circles, but showing that incubation with AM-251 (2 μM) prevented the DSI. (*E*) (*Left*) Plot showing the increased PPR (R2/R1) associated with the DSI shown in *D* (shaded circles) in the six individual cases (open circles) and the corresponding averages (solid circles). (*Upper Right*) Superimposed representative IPSC pairs obtained in experiments as in *D* (shaded circles) in control conditions (solid trace) and the depressed IPSCs 30 min post-ACh (shaded trace). (*Lower Right*) Same IPSCs scaled to the largest response. (*F*) Representative inward current evoked by the ACh pulse at −75 mV during transient interruption of TBS.

modifications of the action currents could be detected by the naked eye (Fig. 1 *B* and *C*). By contrast, when the membrane potential (Vm) was fixed at −75 mV and in the absence of TBS, the ACh pulse induced a persistent reduction of the peak IPSC amplitude to 58 ± 17% of the controls ($P < 0.001$; $N = 6$; Fig. 1*D*, shaded circles). This depression of the IPSC was blocked in the presence of the CB_1R antagonist/inverse agonist [*N*-(piperidin-1-yl)-1-(2,4-dichlorophenyl)-5-(4-iodophenyl)-4-methyl-1H-pyrazole-3-carboxamide] (AM-251) (2 μM), and post-ACh the IPSCs reached values 99 ± 2% those of the controls ($P > 0.05$; $N = 4$; Fig. 1*D*, shaded triangles). Therefore, this depression relied on the activation of CB_1Rs caused by the retrograde action of eCBs liberated from the PC, which decreased the probability of GABA release at inhibitory terminals of CCK^+ interneurons (15). In accordance with a reduction of the GABA release probability during the DSI, the paired-pulse response ratio (PPR, i.e., the quotient of the second R2 over the R1 IPSC) changed from 0.90 or depression (PPD) to 1.43 or facilitation (PPF) ($P < 0.001$; $N = 6$; Fig. 1*E*). A representative example of the inward current evoked by the ACh pulse recorded at −75 mV during transient interruption of TBS is shown in Fig. 1*F*.

Although membrane depolarization itself can potentiate $GABA_A$-mediated responses (16), the TBS protocol alone did not modify IPSCs in the absence of the ACh pulse (Fig. 1*D*, open circles). These results indicate that (*i*) both ACh and membrane depolarization are prerequisites for the induction of the $GABA_A$-LTP and (*ii*) ACh is capable of triggering LTP of synaptic inhibition or the DSI in function of the active or quiescent state of the postsynaptic PC, respectively.

Postsynaptic Mechanisms Dominate the $GABA_A$-LTP. Both pre- and postsynaptic mechanisms can contribute to IPSC potentiation. Therefore, experiments were performed in voltage-clamp conditions with a depolarizing pulse protocol that strongly increases the intracellular Ca^{2+} concentration via influx through voltage-gated Ca^{2+} channels (VGCC). Indeed, such conditions cause both presynaptic effects via the release of eCBs from the PC (15, 17) and postsynaptic effects on $GABA_A$ IPSCs (18). With the repeated 30-s/75-s and 0-mV/−75-mV pulse protocol and the 10-mM Cl^- intracellular solution ($ECl^- = -64.7$ mV), large brief outward IPSCs (166.8 ± 10.1 pA; $N = 6$) were evoked at the 0-mV steps and smaller inward IPSCs (−17.12 ± 3.3 pA; same cells) at −75 mV (Fig. 2 *A* and *B*). Therefore, the responses displayed the properties of $GABA_A$-mediated IPSCs.

During a control depolarizing step there was a gradual decrease of the IPSC amplitude at 0 mV followed by a gradual recovery upon return to −75 mV, indicating that the DSI was evoked (Fig. 2*A*). A modification of the PPR to PPF was evoked by the first depolarizing step (Fig. 2*B*). The ACh pulse induced a gradual enhancement in the IPSC that reached a peak amplitude of 262 ± 18% that of the controls after ∼40 min at the 0-mV steps ($P < 0.001$; $N = 6$; Fig. 2*C*). We transiently interrupted the TBS protocol for ∼5 min and averaged the PPR during the 5 min at −75 mV with paired-pulse stimulation at 0.3 s^{-1}. Mean PPR values were 0.86 in the pre-ACh control and 0.95, 0.99, and 0.98, 10 min, 30 min, and 50 min after the ACh pulse, respectively (Fig. 2*D*). Therefore, the PPR was smaller in the control and tended to increase during the $GABA_A$-LTP ($P < 0.01$; $N = 6$; Fig. 2*D*). This tendency suggests a decreased GABA release probability that persisted throughout the experiment. We tested whether the $GABA_A$-LTP could be induced by repeated briefer 5-s duration depolarizing steps, such as those usually used to evoke the DSI. The 5-s duration depolarizing steps combined with the ACh pulse induced a $GABA_A$-LTP that reached values of 294 ± 40% that of controls ($P < 0.001$; $N = 6$; Fig. 2*E*), essentially identical to those induced by the prolonged 30-s/75-s pulse protocol ($P > 0.05$; $N = 6$ in each case).

$GABA_BRs$ Did Not Contribute to the $GABA_A$-LTP. GABA released by inhibitory interneurons could activate both $GABA_ARs$ and $GABA_BRs$ in CA1 pyramidal neurons. The possible involvement of $GABA_ARs$ was tested and picrotoxin (PiTX) (50 μM) abolished IPSCs (Fig. 3*A*, horizontal shaded bar). We also tested the effects of ACh under blockade of $GABA_BRs$ with the specific $GABA_BR$ antagonist, CGP55845 (2 μM). In these conditions IPSC amplitudes were 230 ± 24% those of the pre-ACh controls ($P < 0.001$; $N = 6$; Fig. 3*B*), not significantly different from when

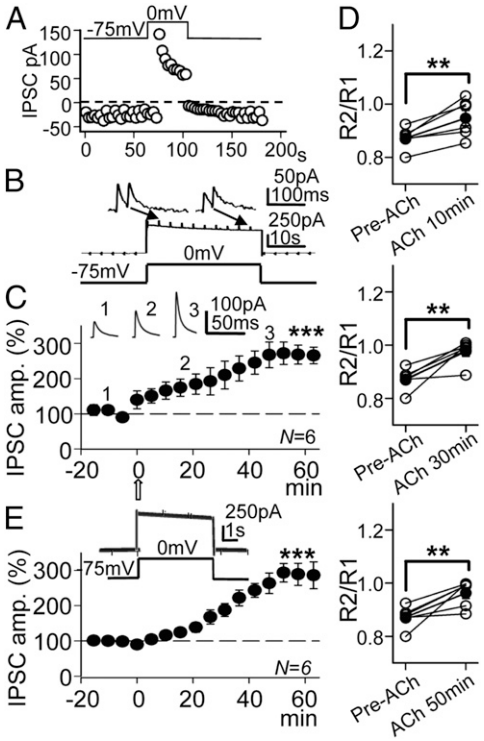

Fig. 2. The $GABA_A$-LTP induced under voltage clamp by ACh and the pulse protocol. (*A*) Temporal evolution of peak IPSC amplitudes during a single depolarizing −75-mV to 0-mV step. A representative experiment shows the DSI and recovery. (*B*) Initial control response evoked by the first depolarizing pulse of the 30-s/0-mV and 75-s/−75-mV protocol and paired-pulse inhibitory stimulation at 0.3/s. (*C*) Plot of the average peak IPSC amplitude vs. time, showing the potentiation induced by ACh recorded at 0 mV. The upper values are IPSC averages from a representative experiment at time points 1, 2 and 3. (*D*) Plot showing the PPR in the six cases (open circles) and the corresponding average (solid circles) computed at the control and 10 min, 30 min, and 50 min post-ACh in the experiments shown in *B*. (*E*) Plot as in *C* showing the $GABA_A$-LTP induced by ACh with the 5-s/15-s pulse protocol shown above.

GABA currents induced by ACh were enhanced in control solution ($P > 0.05$; $N = 6$ in each case, see above). Furthermore, CGP55845 (2 μM) did not modify IPSCS at −75 mV in the absence of ACh and a pulse protocol (Fig. 3*C*). Indeed, the $GABA_B$-mediated IPSCs in CA1 PCs are observed only after postnatal day 22 (19). Therefore, potentiation appeared to be exclusively caused by an increase in the $GABA_A$-mediated responses with no contribution of $GABA_B$Rs.

Presynaptic-Mediated Effects Partially Oppose $GABA_A$-LTP. The data presented above suggest a dominant postsynaptic regulation of the $GABA_A$-LTP. However, the gradual reduction in the IPSC amplitude in the controls and the PPR modifications suggest that presynaptic-mediated effects were also at play throughout the experiment. Therefore, we analyzed the outcome of blocking CB_1Rs with AM-251, first in basal conditions (no pulse protocol and no ACh) that did not modify IPSCs (Fig. 3*D*). By contrast, when the $GABA_A$-LTP had stabilized IPSC amplitudes to 177 ± 13% that of controls ($P < 0.001$; $N = 6$), 2 μM AM-251 increased IPSCs to 273 ± 18% that of controls ($P < 0.01$, $N = 6$; compared with $GABA_A$-LTP and $P < 0.001$, $N = 6$ weighted against the control; Fig. 3*E*). In addition, the PPR changed from 0.86 in the control to 0.96 during the $GABA_A$-LTP ($P < 0.05$; $N = 6$), dropping to 0.74 in the presence of AM-251 (2 μM) ($P < 0.01$; $N = 6$; Fig. 3*F*). These results suggest a presynaptic increase in GABA release probability mediated by the loss of the DSI when CB_1Rs are blocked. Therefore, the $GABA_A$-LTP was augmented slightly because AM-251 blocked the opposing effects of the DSI.

Both the ACh Pulse and Oriens/Alveus Stimulation Persistently Enhanced Inhibitory Postsynaptic Potentials Under Current Clamp. Under current-clamp conditions with blockade of AMPA and NMDA receptors, we tested the effects of the ACh pulse and the TBS protocol in combination with paired-pulse inhibitory stimulation (Fig. 4*A*). With the intracellular solution containing 1 mM Cl^- ($ECl^- = -123.8$ mV), inhibitory postsynaptic potentials (IPSPs) were hyperpolarizations with mean peak amplitudes of −2.6 ± 0.3 mV in control conditions at ∼ −65 mV and 20–22 °C ($N = 8$). The ACh pulse induced a gradual enhancement of the R1 PSPs, which reached a steady state in 20–30 min with amplitudes of 184 ± 29% that of controls [$P < 0.01$; $N = 8$; Fig. 4*B* (*Inset* shows the transient depolarization and action potential burst evoked by the ACh pulse)].

In normal circumstances, ACh is released in the hippocampus by terminals of septal cholinergic fibers running through the *O/A*. In the control conditions, with 10 mM Cl^- intracellular solution ($ECl^- = -64.7$ mV) at 34–36 °C and in the absence of drugs with functional excitatory glutamatergic transmission, the TBS protocol combined with single *O/A* stimulation (duration 10 s,

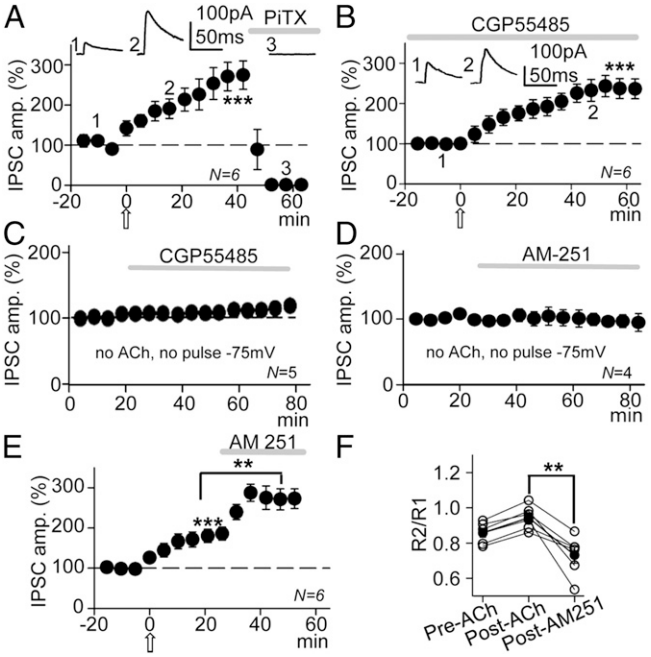

Fig. 3. $GABA_A$Rs but not $GABA_B$Rs mediate the $GABA_A$-LTP that was partially counteracted by a CB_1R-mediated DSI. (*A*) Plot of the average peak IPSC amplitude vs. time, showing that the IPSCs and the $GABA_A$-LTP were abolished by PiTX (50 μM; horizontal shaded bar). The upper values are averaged responses from a representative experiment at time points 1, 2 and 3. (*B*) Plot as in *A*, but showing that blockade of $GABA_B$Rs by incubation with CGP55845 (2 μM) did not interfere with the $GABA_A$-LTP. The upper values are averaged IPSCs from a representative experiment at time points 1 and 2. (*C*) Plot as in *B*, but showing that in the absence of both the pulse protocol and ACh, CGP55845 had no effect on IPSCs recorded at −75 mV. (*D*) Plot as in *B*, but showing that in the absence of the pulse protocol and ACh, AM-251 (2 μM; horizontal bar) had no effect on IPSCs recorded at −75 mV. (*E*) Plot as in *B*, but showing that blockade of CB_1Rs by superfusion with AM-251 (horizontal bar) enhances the $GABA_A$-LTP. (*F*) Plots showing the PPR in the six cases (open circles) and the corresponding average (solid circles) computed at the control, 20 min post-Ach, and post–AM-251 in the experiments shown in *E*.

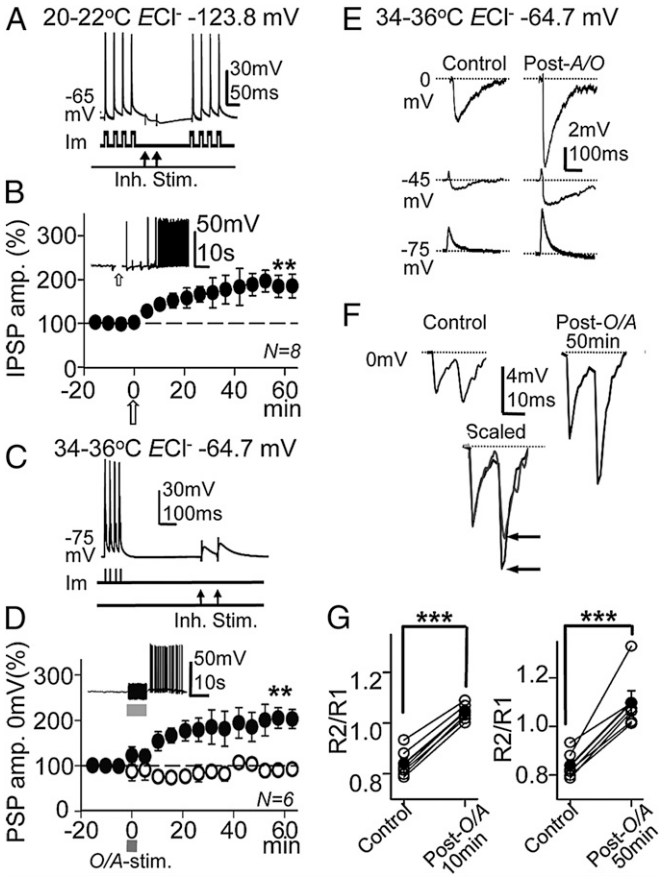

Fig. 4. ACh and stimulation of cholinergic fibers during TBS induced the long-term enhancement of IPSPs. (*A*) Representative current-clamp responses (mV) evoked by the TBS protocol (Im) and paired-pulse inhibitory stimulation (50-ms delay) at the SR (Inh. Stim.). (*B*) Plot of the average peak IPSP amplitude vs. time recorded under current clamp with 1 mM Cl^- intracellular solution ($ECl^- = -123.8$ mV), showing the $GABA_A$-LTP induced by ACh at ~ −65 mV. *Inset* shows a representative response evoked by the ACh pulse during a transient interruption of TBS. (*C*) Same as *A*, but a different PC at −75 mV with paired-pulse stimulation (100-ms delay). (*D*) (solid circles) Same as *B*, but *O/A* stimulation (100 ms, 50 s^{-1}), showing the $GABA_A$-LTP. *Inset* shows a representative response evoked by the *O/A* stimulation. (Open circles) Same as solid circles but under pirenzepine (1 μM). (*E*) Representative responses evoked at 0 mV (IPSP), −45 mV (EPSP-IPSP), and −75 mV (EPSP) in control and post-*O/A* (50 min) conditions. (*F*) (*Upper*) Representative control paired-pulse responses at 0 mV (*Left*) and post-ACh 50 min (*Right*), showing the change in IPSP amplitude and PPR. (*Lower*) Superimposed scaled control and post-ACh IPSPs. Solid and shaded lines, respectively, show the change to PPF (horizontal arrows). (*G*) Plots showing the PPR in the six cases (open circles) and the corresponding average (solid circles) computed at the control and 10 min and 50 min post-*O/A* in the experiments shown in *D* (solid circles).

frequency 50 s^{-1}) current clamped at −75 mV (Fig. 4*C*) induced a slow depolarization and an action potential burst (Fig. 4*D*, *Inset*). Responses evoked by single- or paired-pulse inhibitory stimulation at 0 mV, −45 mV, and −75 mV were mainly composed of hyperpolarizing IPSPs, biphasic dehyperpolarizing excitatory postsynaptic potential (EPSP)–IPSP sequences, and depolarizing EPSPs, respectively (Fig. 4 *E* and *F*). Following *O/A* stimulation, the synaptic responses at 0 mV, −45 mV, and −75 mV increased in amplitude. At 0 mV, *O/A* stimulation induced a strong potentiation of IPSP peak amplitudes that reached a steady state of 182 ± 19% that of the controls within 20–30 min ($P < 0.01$; $N = 6$; Fig. 4*D*, solid circles). Moreover, incubation with the specific M1-mAChR antagonist pirenzepine (1 μM) prevented this $GABA_A$-LTP from developing, whereby the IPSPs recorded before and after *O/A* stimulation were essentially identical and reached 97 ± 6% of the control value ($P > 0.05$; $n = 6$; Fig. 4*D*, open circles). In addition, paired-pulse responses changed from PPD to PPF (Fig. 4*F*). The mean PPR value in the pre-ACh control was 0.83, and it was 1.04 and 1.09, 10 and 50 min after stimulation, respectively. Therefore, the PPR was smaller in the control and it increased during $GABA_A$-LTP ($P < 0.001$; $N = 6$; Fig. 4*G*), suggesting a lower probability of GABA release. In these conditions EPSPs were also potentiated (Fig. 4*E*), a result in agreement with our previous reports (4, 5).

ACh Acts Through M1-mAChR Activation. ACh could induce $GABA_A$-LTP by activating mAChRs and/or nAChRs. Therefore, we tested the influence of mAChRs, using the wide spectrum mAChR antagonist atropine (0.3 μM), the specific M1-mAChR antagonist pirenzepine (1 μM), and the specific M2-mAChR antagonist methoctramine (2 μM). Both atropine and pirenzepine blocked $GABA_A$-LTP, and control and post-ACh IPSCs were essentially identical in the presence of these antagonists (Fig. 5*A*), with IPSCs reaching 95 ± 3% and 100 ± 14% the control value in the presence of atropine ($P > 0.05$; $N = 6$) and pirenzepine ($P > 0.05$; $N = 7$), respectively. Moreover, in the presence of methoctramine the $GABA_A$-LTP reached values of 203 ± 8% that of the basal value ($P < 0.001$; $N = 6$; Fig. 5*A*), essentially identical to the $GABA_A$-LTP evoked in control conditions ($P > 0.05$; $N = 6$).

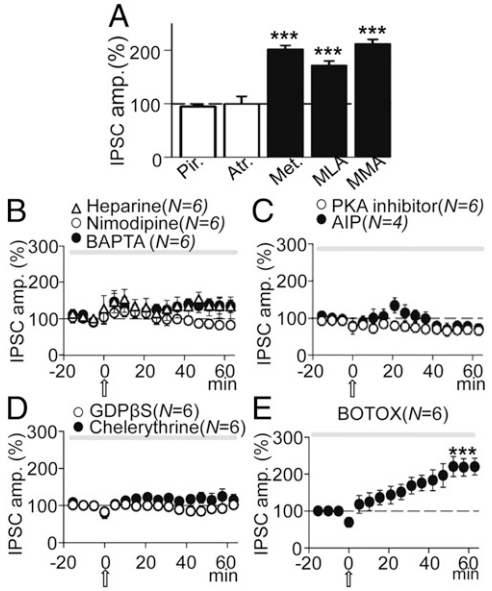

Fig. 5. The $GABA_A$-LTP required activation of M1-mAChRs, an increased cytosolic Ca^{2+}, and activation of various intracellular cascades. (*A*) Pooled data showing the effects of blocking AChRs by incubation with pirenzepine (Pir.; 1 μM; $N = 7$), atropine (Atr.; 0.3 μM; $N = 6$), methoctramine (Met.; 2 μM; $N = 6$), methyllycaconitine (MLA.; 125 μM; $N = 6$), and mecamylamine (MMA.; 10 μM; $N = 6$) on the peak amplitude of IPSCs recorded 50 min post-ACh. Data were expressed as the percentage change from baseline, where 100% (dashed line) is the average peak amplitude value of the control IPSCs for each respective condition. (*B*) Superimposed IPSC amplitude vs. time plots, showing the effects of incubation with Heparin (5 mg/mL; triangles; $N = 6$) and Nimodipine (10 μM; open circles; $N = 6$) and of BAPTA loading (20 mM; solid circles). (*C*) Same as *B*, but showing the effects of intracellular loading with the PKA inhibitor (10 μM; open circles; $N = 4$) and AIP (10 μM; solid circles; $N = 6$). (*D*) Same as *B*, but showing the effects of intracellular loading with, GDPβS (2 mM; open circles; $N = 6$) and Chelerythrine (2 μM; solid circles; $N = 6$). (*E*) Same as *B*, but showing the absence of effects of intracellular loading with BOTOX (0.5 μM; $N = 6$).

We also tested the effects of antagonizing both the α7-nAChR with methyllycaconitine (MLA) (125 μM) and the non–α7-nAChR with mecamylamine (MMA) (10 μM). Neither of these two antagonists affected the $GABA_A$-LTP, which reached 180 ± 8% the basal value ($P < 0.001$; $N = 6$) in the presence of MLA and 217 ± 11% the basal value in the presence of MMA ($P < 0.001$; $N = 6$; Fig. 5*A*). Hence, nAChRs did not appear to contribute to IPSC potentiation and MLA and MMA did not modify control IPSCs ($P > 0.05$; $N = 4$ in each case).

The $GABA_A$-LTP Required a Rise in Intracellular Ca^{2+}. Calcium is usually involved in the induction of long-term synaptic plasticity (20) and can regulate the release of eCBs and modify the surface expression of $GABA_A$ channels (see below). Therefore, we tested the effects of chelating Ca^{2+} through 1,2-bis (0-aminophenoxy) ethane-*N*,*N*,*N*′,*N*′-tetraacetic acid (BAPTA) loading (20 mM in the pipette solution), thereby inhibiting its intracellular effects. Intracellular BAPTA blocked the $GABA_A$-LTP, and pre- and post-ACh IPSCs were essentially identical (109 ± 7%; $P > 0.05$; $N = 6$; Fig. 5*B*, solid circles). In our experimental conditions, an increase in Ca^{2+} may be brought about by an influx via L-type VGCCs that may influence $GABA_A$R expression and synaptic inhibition (18) or due to release from IP_3-sensitive endoplasmic reticulum stores (5). Therefore, we tested the effects of blocking L-type VGCC with nimodipine (10 μM) and of inhibition of IP_3 receptors (IP_3Rs) by intracellular loading with heparin (5 mg/mL). Nimodipine blocked the $GABA_A$-LTP and reduced IPSCs that reached values of 79 ± 8% that of controls ($P > 0.05$; $N = 6$; Fig. 5*B*, open circles), whereas intracellular heparin markedly reduced the $GABA_A$-LTP to values of 122 ± 5% that of controls ($P < 0.05$; $N = 6$; Fig. 5*B*, triangles). Therefore, a postsynaptic rise in the intracellular Ca^{2+} concentration appeared to be fundamental to generate the $GABA_A$-LTP.

The Signaling Pathways Contributing to the $GABA_A$-LTP. G-protein–coupled receptors, PLC, calcium calmodulin kinase II (CaMKII), PKC, and PKA activities triggered by Ca^{2+}-dependent mechanisms are known to participate in inducing the long-term potentiation of excitatory synaptic transmission mediated through activation of M1-mAChRs in CA1 pyramidal neurons (4, 5). Thus, the same intracellular cascades could participate in the induction of the $GABA_A$-LTP. However, the requirement of depolarization is an important difference between these processes and indeed, depolarization may strongly increase intracellular Ca^{2+} and thereby activate other intracellular routes (21). Accordingly, we assessed the effects of including the nonpermeable PKA inhibitor (10 μM) in the pipette solution and found it to depress IPSCs to 74 ± 5% that of controls ($P < 0.01$; $N = 6$; Fig. 5*C*, open circles). We also tested the effects of the CaMKII inhibitor, AIP (10 μM), included in the pipette solution, and following an initial potentiation that 20 min after the ACh challenge reached values of 122 ± 3%, this decayed rapidly and depressed IPSCs to 71 ± 3% of the controls ($P < 0.01$; $N = 4$; Fig. 5*C*, solid circles).

We investigated the contribution of G-protein–coupled receptors to the $GABA_A$-LTP by blocking G proteins through the inclusion of GDPβS in the pipette solution. GDPβS (2 mM) abolished the $GABA_A$-LTP (post-ACh IPSCs reached values of 106 ± 6% of controls; $P > 0.05$; $N = 6$; Fig. 5*D*, open circles), indicating that G-protein activation was essential for the induction of the $GABA_A$-LTP. By contrast, GDPβS did not modify control IPSCs ($P > 0.05$; $N = 3$). Both PKC and PKA activation can regulate $GABA_A$-mediated currents (22, 23) and participate in the induction of long-term synaptic plasticity at both inhibitory and excitatory synapses (16, 22–24). Therefore, we tested the effects of inhibiting PKC by including chelerythrine (2 μM) in the pipette solution, which reduced the $GABA_A$-LTP that reached values of 120 ± 6% that of controls ($P < 0.05$; $N = 6$; Fig. 5*D*, solid circles). Together these results suggest that the $GABA_A$-LTP requires postsynaptic signaling pathways that involve interaction of Ca^{2+} with G proteins, CaMKII, and PKA, with a contribution from PKC.

$GABA_A$Rs Were Not Transported to the Synapse by Endosomes. Postsynaptic modifications in the efficacy of $GABA_A$ inhibition usually occur as a result of changes in receptor number at the synapse (25). Therefore, we tested whether $GABA_A$-LTP relied on an increase in the number of new $GABA_A$Rs introduced to the synapse by endosomes. When the pipette solution included the B-type botulinum toxin BOTOX (0.5 μM), which inhibits SNARE protein-mediated membrane fusion of endosome complexes, $GABA_A$-LTP was induced and IPSC amplitudes reached values of 194.5 ± 7% the basal levels ($P < 0.001$; $N = 6$; Fig. 5*E*), essentially identical to the values reached in control conditions ($P > 0.05$; $N = 6$). Therefore, the number of $GABA_A$ receptors at the synapse did not appear to increase as a result of the insertion of new $GABA_A$Rs transported by endosomes (26).

We had previously shown that BOTOX loading prevented the LTP of glutamatergic transmission induced by ACh in CA1 PCs. We checked whether BOTOX was working in experiments with functional excitatory transmission and synaptic inhibition blocked by PiTX (50 μM). In these conditions BOTOX loading prevented the ACh-induced LTP of the excitatory synaptic transmission (4) and control and post-ACh excitatory postsynaptic currents (EPSCs) were essentially identical ($P > 0.05$; $N = 5$; Fig. S1), indicating that BOTOX was in fact inhibiting SNARE protein-dependent membrane fusion of endosomes. In addition, BOTOX did not block the LTP of the NMDA component of EPSCs (4) (Fig. S1).

The $GABA_A$-LTP Was Paralleled by an Increased Contribution of $\alpha_5\beta\gamma_2$ Subunit-Containing Receptors. The $GABA_A$-LTP could be the result of an increase in the number of synaptic $GABA_A$Rs possibly caused by the lateral diffusion into the synapse of extrasynaptic $GABA_A$Rs. The $\alpha_5\beta\gamma_2$ subunit-containing $GABA_A$ receptors ($\alpha_5\beta\gamma_2$-$GABA_A$Rs) are typified by their high sensitivity to GABA and slow decay kinetics, and they concentrate at extrasynaptic locations in CA1 PCs, thereby providing a modest contribution to transient inhibition in control conditions (27, 28). Accordingly, a gradual increase in the IPSC amplitude and a decrease of the decay slope could be expected if the $GABA_A$-LTP is the outcome of the lateral diffusion into the synapse of extrasynaptic $\alpha_5\beta\gamma_2$-$GABA_A$Rs. Indeed, the IPSC decay tau (T) increased gradually during the $GABA_A$-LTP from a mean control T of 31 ± 1 ms to 49 ± 2 ms (a 160 ± 9% increase from controls; $P < 0.001$; $N = 6$; Fig. 6 *A* and *B*).

The sustained GABA current that causes the tonic inhibition is mediated through $\alpha_5\beta\gamma_2$-$GABA_A$Rs (29) and therefore it should be enhanced with the $GABA_A$-LTP. The difference between the average control pre-ACh holding current and the average holding current associated with the IPSC potentiation at −75 mV provides a measure of the tonic GABA current. The average holding current was −79 ± 4 pA in control conditions and dropped to −39 ± 7 pA with the IPSC potentiation or 50 ± 5% of the control value ($P < 0.001$; $N = 6$; Fig. 6*C*). Hence, more $\alpha_5\beta\gamma_2$ $GABA_A$Rs would appear to be activated by the released GABA.

The aforementioned increase in the decay T of IPSCs could indicate an increase in the activation of $\alpha_5\beta\gamma_2$-$GABA_A$Rs. Hence, we superfused L-655,708 a nootropic drug that at low nanomolar concentrations is an inverse agonist of $\alpha_5\beta\gamma_2$-$GABA_A$Rs (29). When the $GABA_A$-LTP had stabilized, L-655,708 (20 nM) induced a marked reduction of the peak IPSC amplitude from 237 ± 27% ($P < 0.01$; $N = 6$; Fig. 6*D*) to 131 ± 36% (a 105 ± 13% reduction; $P < 0.01$, same cells; Fig. 6*D*). Matching the $GABA_A$-LTP, there was an initial increase of the

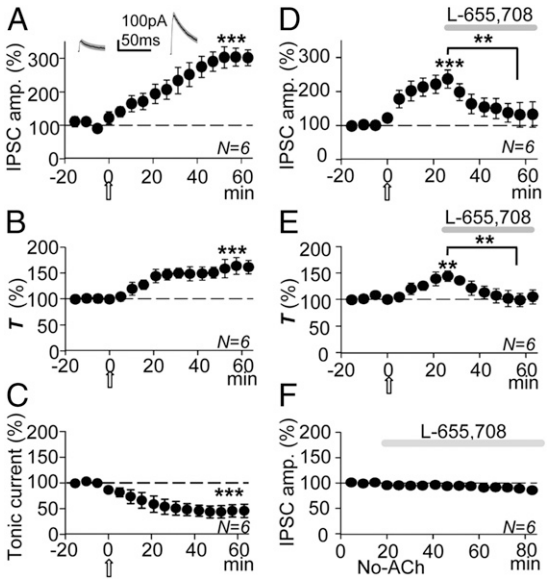

Fig. 6. The $GABA_A$-LTP was matched by a decreased IPSC decay slope and an increased tonic GABA current and markedly reduced by blockade of $\alpha_5\beta\gamma_2$-$GABA_A$Rs. (*A*) Plot of the average peak IPSP amplitude vs. time, showing the $GABA_A$-LTP. *Insets* show representative average control (*Left*) and potentiated IPSCs (*Right*) and single exponential fits (thin solid and thick shaded superimposed traces, respectively). (*B*) Same as *A*, but plot of average *T* values (percentage of control, as in all other cases) vs. time, showing the increased *T* paralleling the $GABA_A$-LTP. (*C*) Plot of average tonic GABA current values (percentage of control at −75 mV) vs. time, showing the gradual change in tonic GABA current associated with the $GABA_A$-LTP. GABA currents (as IPSCs) were negative at −75 mV. *A*–*C* show data from the same six experiments. (*D*) Same as *A*, but showing the $GABA_A$-LTP and the marked IPSC reduction induced by superfusion with L-655,708 (20 nM; horizontal shaded bar). (*E*) Same as *B*, but showing the increased *T* paralleling the $GABA_A$-LTP and its reduction by L-655,708. Data are taken from *D*. (*F*) With the pulse protocol but in the absence of ACh, L-655,708 induced a small, not significant IPSC reduction.

decay *T* of IPSCs (a 144 ± 10% increase of that of the controls; $P < 0.01$; $N = 6$; Fig. 6*E*) that dropped to 105 ± 13% of the control value during the subsequent L-655,708–induced reduction in the IPSC amplitude ($P < 0.01$; $N = 6$; Fig. 6*E*). Significantly, in the absence of the ACh pulse, superfusion with L-655,708 (20–50 nM) did not modify the IPSC amplitudes (94 ± 5% that of the controls; $P > 0.05$; $N = 6$; Fig. 6*F*), suggesting that an insignificant number of $\alpha_5\beta\gamma_2$-$GABA_A$Rs were being activated by the GABA released in the absence of mAChR activation.

The IPSCs Voltage Dependence Acquired During the $GABA_A$-LTP Was Prevented by Blocking $\alpha_5\beta\gamma_2$-$GABA_A$Rs. Outward rectification and a higher GABA sensitivity are hallmarks of $\alpha_5\beta\gamma_2$-$GABA_A$Rs (30). Therefore, we asked whether the $GABA_A$-LTP was paralleled by an increase in the slope conductance and outward rectification of IPSCs. We used the same ACh pulse and 30-s/75-s pulse protocol to induce the $GABA_A$-LTP, measuring the IPSC voltage sensitivity with I/V relationships at a holding potential of 0 mV, while the pulse protocol was interrupted, during the establishment of the $GABA_A$-LTP, and when the potentiation had stabilized. The I/V protocol involved 500-ms duration, 10-mV voltage control steps from −100 mV to +20 mV, applied every 5 s, while the inhibitory fibers were stimulated with a single pulse (Fig. 7 *C* and *F*, *Insets*). The small IPSCs evoked in control conditions and the larger IPSCs evoked when the $GABA_A$-LTP had stabilized are shown in Fig. 7 *A* and *B*, respectively. The control I/V relationships of peak IPSC amplitudes were linear with small average slopes (Fig. 7*C*, solid circles), whereas there was an increase of the slope conductance as the $GABA_A$-LTP progressed and the emergence of a strong outward rectification of IPSCs above ~ −50 mV (Fig. 7*C*, Post-ACh). We calculated a rectification index (RI) of IPSCs as a ratio of slopes from peak IPSC values (IPSC) at −60 mV, 0 mV, and +20 mV from I/V relationships, where

$$\text{slope 1} = \frac{(\text{IPSC} - 60\ \text{mV}) - (\text{IPSC}\ \ 0\ \text{mV})}{\text{IPSC} - 60\ \text{mV}}$$

$$\text{slope 2} = \frac{(\text{IPSC}\ \ 0\ \text{mV}) - (\text{IPSC} + 20\ \text{mV})}{\text{IPSC} + 20\ \text{mV}}$$

$$\text{RI} = \frac{\text{slope 2}}{\text{slope 1}}.$$

The control RI and the evolution of RI values in control solution plotted as a function of time after the ACh pulse are shown in Fig. 7*G* (solid circles). The gradual enhancement of both slope conductance and outward rectification supports the view that the $GABA_A$-LTP is caused by a regular increase in the number of $\alpha_5\beta\gamma_2$-$GABA_A$Rs activated by the released GABA. We also measured I/V relationships of potentiated IPSCs at delays of 20 ms from the peak current in the same cells. Accordingly, we found no significant differences in the I/V relationships calculated with peak IPSC values ($P > 0.05$; $N = 6$). This result differs somewhat from the rectification found at delays >20 ms from the stimulation (30), a discrepancy that could be due to the different recording and stimulation conditions or to the use of older animals.

Taken together, the data obtained suggest a major contribution of $\alpha_5\beta\gamma_2$-$GABA_A$Rs to the $GABA_A$-LTP and indeed, L-655,708 (20 nM) prevented the $GABA_A$-LTP and reduced the IPSC amplitudes (Fig. 7 *D* and *E*). I/V relationships reveal that L-655,708 also inhibited the increase in slope conductance and outward rectification of IPSCs (Fig. 7*F*). The control pre-ACh RI and the RI measured 60 min post-ACh under blockade of $\alpha_5\beta\gamma_2$-$GABA_A$Rs with L-655,708 (20 nM) are shown in Fig. 7*G* (open circles). Thus, $GABA_A$-LTP appears to be caused by an increase in the number of L-655,708–sensitive $\alpha_5\beta\gamma_2$-$GABA_A$Rs activated by the GABA released.

The Cl^- Driving Force, Concentration Gradient, and K^+ Conductance Did Not Contribute to the $GABA_A$-LTP. Changes in the intra/extracellular Cl^- concentration gradient caused by Cl^- flux through activated $GABA_A$Rs may globally modify $GABA_A$-mediated synaptic activity, an effect that can be aided by activity-dependent changes in Cl^- transporter function (31, 32). With the 10-mM Cl^- solution ($ECl^- = -64.7$ mV), the $GABA_A$-LTP reached values of 299 ± 38% those of the controls ($P < 0.001$; $N = 6$) when recorded at the 0-mV steps (Fig. S2*A*) and of 241 ± 30% those of the controls ($P < 0.001$, same cells) when recorded at −75 mV (Fig. S2*B*). Therefore, the $GABA_A$-LTP magnitude was larger at 0 mV than at −75 mV ($P < 0.05$, same cells). We also tested the effects of blocking K^+-mediated conductances under voltage-clamp conditions, with the Cs^+-based 110-mM intracellular Cl^- solution ($ECl^- = -3.9$ mV). In these conditions, the $GABA_A$-LTP induced by ACh with the 30-s/75-s pulse protocol and measured at 0 mV stabilized at amplitudes of 269 ± 10% the control value ($P < 0.001$; $N = 7$; Fig. S2*C*). This IPSC enhancement was comparable to that induced with the 10-mM intracellular Cl^- solution ($P > 0.05$; $N = 7$). The magnitude of the $GABA_A$-LTP achieved with different intracellular Cl^- concentrations and Vms is shown in Fig. S2*D*.

Effects of the Timing and Duration of the Stimulation Protocol. Because the $GABA_A$-LTP is different from other LTPs, it was relevant to test whether the $GABA_A$-LTP persisted when protocols were interrupted following its induction. Interrupting the

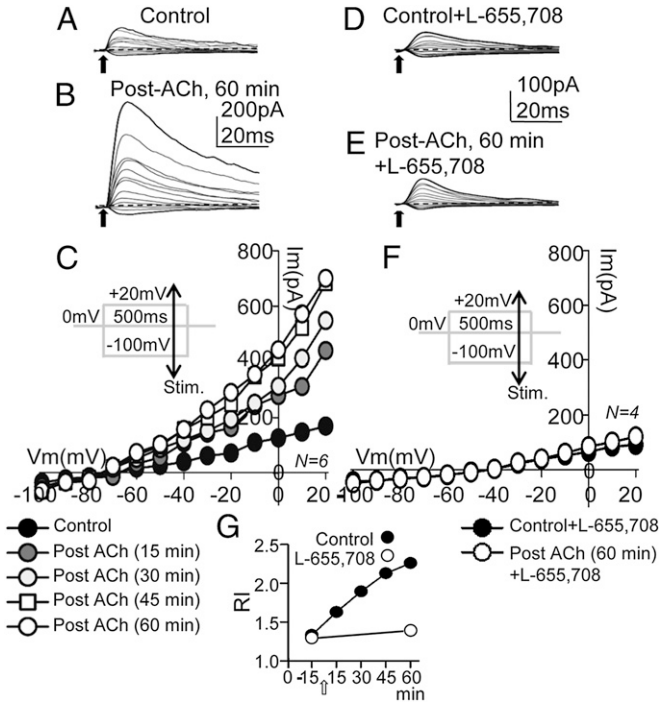

Fig. 7. An increased slope conductance and outward rectification of IPSCs were associated with the $GABA_A$-LTP. (*A*) Representative control IPSCs recorded during 10-mV voltage-control steps from −100 mV to +20 mV at a holding potential of 0 mV (see protocol in *C*). (*B*) Same as *A*, but post-ACh, 60 min showing potentiated IPSC, especially at depolarized Vms. (*C*) I/V relationships calculated with peak IPSC amplitudes in control conditions and at increasing times after the ACh pulse. The control I/V relationship tends to linear (solid circles), whereas the average slope conductance and outward rectification increase gradually with time after ACh. Note the unchanged reversal potential. (*D* and *E*) Same as *A* and *B*, but under superfusion with L-655,708 (20 nM). Note the similar IPSC amplitudes in *D* and *E* and the faster decay slopes in *E*. (*F*) Same as *C*, but control plus L-655,708 (solid circles) and post-ACh (60 min) plus L-655,708, showing the IPSC reduction and the absence of outward rectification under blockade of $\alpha_5\beta\gamma_2$-$GABA_A$Rs. (*G*) Plot showing the temporal evolution of RI values in control solution (solid circles) and under L-655,708 (open circles) in the pre-ACh control and 60 min post-ACh (open arrow).

30-s/75-s pulse protocol during ∼20 min did not prevent the $GABA_A$-LTP that reached values 230 ± 18% those of the controls ($P < 0.001$; $N = 6$; Fig. S3*A*). Moreover, suspending the inhibitory stimulation for ∼20 min did not hinder the $GABA_A$-LTP that reached values of 233 ± 16% those of the controls ($P < 0.001$; $N = 6$; Fig. S3*B*). In both cases, the magnitude of the $GABA_A$-LTP was essentially identical to that induced in control conditions ($P < 0.05$; $N = 6$). Interestingly, when the 30-s/75-s depolarizing pulse protocol was applied throughout the pre-ACh control and it was interrupted 10 min after the ACh pulse, a transient IPSC potentiation was induced that peaked ∼10 min after the ACh pulse and that reached values of 203 ± 21% of the control value ($P < 0.01$; $N = 6$; Fig. S3*C*). This potentiation decayed to the basal sate within ∼40 min and a single 30-s/75-s depolarizing step to 0 mV applied ∼18 min later did not modify IPSCs amplitudes. Together these data suggest that following the ACh challenge the repeated depolarizing protocol induces a buildup of the intracellular machinery that ultimately stabilizes the expression of the $GABA_A$-LTP.

Contribution of CCK^+ and PV^+ Interneurons to $GABA_A$-LTP. Electrical stimulation in the SR, close to the soma of the recorded PC, can trigger simultaneous GABA release from CCK^+ and PV^+ interneurons (33, 34). To estimate the relative contribution of CCK^+ and PV^+ interneurons to $GABA_A$-LTP, we superfused ω-conotoxin GVIA (ω-CgTx) to specifically and irreversibly inhibit the N-type VGCCs that control GABA release from the axon terminals of CCK^+ interneurons (35). When ω-CgTx (0.5 μM) was applied when $GABA_A$-LTP had reached a steady state (established as 100% the baseline), it induced a strong reduction of the IPSCs from the previously potentiated IPSC amplitude values (59 ± 4%, $P < 0.001$; $N = 6$; Fig. S3*D*). We also superfused PCs with ω-agatoxin (ω-Aga), which specifically inhibits the P/Q-type VGCCs that control GABA release from the axon terminals of PV^+ interneurons. The presence of ω-Aga (250 nM), applied when the $GABA_A$-LTP had reached a steady state, induced a reduction of 37 ± 4% ($P < 0.001$; $N = 6$; Fig. S3*E*) from the previously potentiated values. The reduction in IPSC induced by ω-CgTx was stronger than that induced by ω-Aga ($P < 0.01$; $N = 6$ in each case).

Discussion

We describe a form of long-lasting postsynaptic enhancement of $GABA_A$ inhibition in CA1 pyramidal neurons that we term $GABA_A$-LTP. The $GABA_A$-LTP combines effects of a transient activation of M1-mAChRs and repeated postsynaptic depolarization, presenting a key difference with the rebound potentiation of IPSCs in Purkinje neurons that requires only postsynaptic depolarization (16). The $GABA_A$-LTP also differs from the inhibitory LTP in nucleus *tractus solitarii* neurons, which is blocked by $GABA_B$-receptor antagonists (36). The $GABA_A$-LTP is not paralleled by changes in the Cl^- reversal potential, as occurs in other forms of potentiation of $GABA_A$ synapses (31, 32), and is also unrelated to to the presynaptic enhancement of GABA transmission in hippocampal neuronal and slice cultures (37). Interestingly, similar induction protocols also induce long-term changes at excitatory synapses in CA1 PCs (4, 5) but the functional impact of pairing muscarinic receptor activation and pyramidal cell firing remains untested.

Pre- and Postsynaptic Components Are Involved in the $GABA_A$-LTP. We show that in the absence of membrane depolarization ACh generates a CB_1R-dependent DSI. This effect reveals that postsynaptic activity gates the effects of ACh on inhibition from a presynaptic locus, whereby a DSI was induced to a postsynaptic site of dominance where the $GABA_A$-LTP was triggered. The CB_1Rs-dependent DSI described here displays a crucial divergence from the long-term depression at inhibitory synapses induced by activation of metabotropic glutamate receptor or mAChR, which rapidly becomes insensitive to CB_1R antagonists (11, 13, 38). Indeed, because it is induced by the prolonged presentation of repeated depolarization, it could be related with eCB-DSI (13). In addition, this DSI was eliminated by the muscarinic antagonist atropine, suggesting that mAChR activation contributed to the DSI. Importantly, cholinergic activity may depress IPSCs through endocannabinoid release (12, 39), suggesting that the CB_1R-dependent eCB-DSI could contribute to the DSI described here.

The effects of blocking GABA release from CCK^+ and PV^+ interneurons suggest that although both types of interneuron contribute to the $GABA_A$-LTP, CCK^+ interneurons appear to be more strongly involved in this phenomenon (34).

An Intracellular Ca^{2+} Rise Is Required to Induce the $GABA_A$-LTP. The $GABA_A$-LTP was suppressed by sequestering Ca^{2+} and counteracting its intracellular effects and by inhibiting L-type VGCC and depolarization-dependent Ca^{2+} influx. Hence, membrane depolarization appears to play an important role in the intracellular rise in Ca^{2+} and in the induction of the $GABA_A$-LTP. Intracellular heparin prevents Ca^{2+} release from IP_3-sensitive endoplasmic reticulum stores and dampens the $GABA_A$-LTP. Therefore, the $GABA_A$-LTP was linked to an increase of the intracellular Ca^{2+} concentration due to an influx via L-type VGCC aided by Ca^{2+} release from IP_3-sensitive stores. Interestingly,

similar mechanisms are at play in the LTP of excitatory synapses in CA1 PCs (4, 5).

An Increased Contribution of $\alpha_5\beta\gamma_2$-Containing $GABA_A$Rs to the IPSCs Mediates the $GABA_A$-LTP. Synaptically released GABA saturates $GABA_A$Rs; therefore, we propose that postsynaptic increases in the efficacy of $GABA_A$ inhibition could result from a rise in receptor number at the synapse (25, 40, 41), possibly compounded by the lateral diffusion into the synapse of preexisting extrasynaptic $GABA_A$Rs (26, 42, 43). Our data could suggest that the $GABA_A$-LTP is associated with a Ca^{2+}-triggered increase in the number of $\alpha_5\beta\gamma_2$-$GABA_A$Rs that sense the GABA released (23, 43). Indeed, several traits of the $GABA_A$-LTP support this possibility, as it (*i*) was not induced by insertion of new $GABA_A$Rs transported by endosomes, (*ii*) is typified by an increased decay *T* that characterizes $\alpha_5\beta\gamma_2$-containing $GABA_A$Rs-mediated IPSCs (27, 40), (*iii*) is paralleled by an enhanced slope conductance and outward rectification that differentiates $\alpha_5\beta\gamma_2$-$GABA_A$Rs (44), (*iv*) is matched by the sustained current that mediates the $\alpha_5\beta\gamma_2$-$GABA_A$Rs-dependent tonic inhibition (29, 44–46), and (*v*) is blocked by low nanomolar concentrations of L-655,708 that specifically antagonizes $\alpha_5\beta\gamma_2$-$GABA_A$Rs (46). However, we did not demonstrate directly that extrasynaptic $GABA_A$Rs migrate to the synapse, a mechanism that to our knowledge has been unequivocally demonstrated only in neuronal cultures (37).

We show that the effect of L-655,708 was negligible in the controls, probably indicating that the naive synapses were in a non–$GABA_A$-LTP state. By contrast, the effect of L-655,708 was strong during the $GABA_A$-LTP, supporting the notion that it is at least partially driven by more $\alpha_5\beta\gamma_2$-$GABA_A$Rs sensing the GABA released. The strong increase in slope conductance caused by the stronger contribution of $\alpha5\beta\gamma2$-$GABA_A$Rs could explain the robust change in the average holding current (i.e., the sustained GABA current) during the $GABA_A$-LTP and the powerful IPSP/IPSC potentiation associated with the $GABA_A$-LTP. Interestingly, under voltage clamp the $GABA_A$-LTP was significantly stronger at 0 mV than at −75 mV, a feature consistent with the enhanced contribution of the vigorous outward rectification that typifies $\alpha_5\beta\gamma_2$-$GABA_A$Rs and that is absent from naive synapses.

Synapses expressing $\alpha_5\beta\gamma_2$-$GABA_A$Rs are mainly localized in the dendrites of CA1 PCs (46) and phasic inhibition through $\alpha5\beta\gamma2$-$GABA_A$Rs occurs through dendrite-preferring interneurons in the cortex of young rats (47). The absence of a significant contribution of $\alpha_5\beta\gamma_2$-$GABA_A$Rs in naive synapses could indicate that we were preferentially activating perisomatic inhibition, whereas dendritic synapses that contain $\alpha_5\beta\gamma_2$-$GABA_A$Rs (47, 48) did not contribute considerably to the IPSCs. However, we cannot reject a possible contribution of dendritic synapses because the stimulation in the SR could activate both perisomatic and proximal dendritic inhibition.

The Ca^{2+} Rise Activates Kinase Pathways That Trigger the $GABA_A$-LTP. The strong Ca^{2+} elevation induced by M1-mAChR activation and depolarization could stimulate PKC and CAMKII. These kinases are involved in synaptic plasticity and they are required to induce the $GABA_A$-LTP and could regulate the incorporation of $\alpha5\beta\gamma2$-$GABA_A$Rs into synapses. Inhibition of PKA induces a postsynaptic reduction in IPSC amplitudes and it regulates the GABA release probability, suggesting pre- and postsynaptic contributions to the $GABA_A$-LTP. In this scenario, the $GABA_A$-LTP could operate as a homeostatic negative feedback mechanism to control abnormal hyperexcitable states in the CA1 network, thereby preventing strong detrimental Ca^{2+} influx.

A possible mechanism to explain our data could involve PKA activation through Ca^{2+}/calmodulin-stimulated adenylyl cyclase (2), independent of M2-mAChR activation. This would explain the requirement for both depolarization and M1-mAChR activation to reach the necessary cytosolic Ca^{2+} to activate adenylyl cyclase. In this scenario the Ca^{2+}/calmodulin-stimulated adenylyl cyclase would act as a coincidence detector for the induction of the $GABA_A$-LTP.

"Spillover" and the $GABA_A$-LTP. An alternative possibility that might explain the $GABA_A$-LTP is that more extrasynaptic $\alpha_5\beta\gamma_2$-containing $GABA_A$Rs are activated by GABA spillover and mediate the $GABA_A$-LTP. Spillover could result from enhanced GABA release or diminished GABA uptake. Although we cannot provide a direct demonstration that spillover contributes to the $GABA_A$-LTP, it appears unlikely because (*i*) the $GABA_A$-LTP was paralleled by a decreased GABA release probability associated with a CB_1R-dependent eCB-DSI, an effect that would reduce spillover; (*ii*) raising the bath temperature did not modify the $GABA_A$-LTP, whereas spillover is strongly influenced by temperature due to enhanced GABA uptake; and finally, (*iii*) blocking $GABA_B$R had no effect on the $GABA_A$-LTP, even though presynaptic inhibition through $GABA_B$R at interneuron terminals has been shown to reduce GABA release by blocking VGCCs (48).

Materials and Methods

Procedures for animal care and slice preparation were approved by the Consejo Superior de Investigaciones Científicas, in accordance with the guidelines of the European Council on the ethical use of animals (Directive 2010/63/EU) and with every effort being made to minimize the suffering and number of animals used. Most of the procedures have been described in detail elsewhere (4, 5).

Slice Preparation. Young Wistar rats of either sex (14–20 d) were decapitated, and the brain was removed and submerged in cold (~4 °C) artificial cerebrospinal fluid (ACSF) that contained 124 mM NaCl, 2.69 mM KCl, 1.25 mM KH_2PO_4, 2 mM $MgSO_4$, 26 mM $NaHCO_3$, 2 mM $CaCl_2$, 10 mM glucose, and 0.40 mM ascorbic acid. The pH was stabilized at 7.4 by bubbling carbogen through the solution [95% (vol/vol) O_2, 5% (vol/vol) CO_2]. Transverse hippocampal Vibratome slices (300–400 μm thick; Pelco 3000) were incubated in ACSF >1 h at a room temperature of 20–22 °C. Slices were transferred to a 2-mL chamber fixed to an upright microscope (Olympus BX51WI) equipped with infrared differential interference contrast video microscopy (DIC) and a 40× water immersion objective. Slices were superfused (2 mL/min) with ACSF bubbled with carbogen. Recordings were obtained with the blockade of glutamatergic ionotropic transmission in the presence of 2-amino-5-phosphonopentanoic acid (D-AP5; 50 μM) to inhibit NMDA receptors (NMDARs) and 7-nitro-2, 3-dioxo-1, 4-dihydroquinoxaline-6-carbonitrile (CNQX; 20 μM) to block AMPA receptors (AMPARs), except in Fig. 4 *C–G* and Fig. S1. The following drugs were added to the ACSF as needed: atropine (0.3 μM), pirenzepine (1 μM), methoctramine (2 μM), L-655,708 (20–50 nM), PiTX (50 μM), bicuculine (50 μM), CGP55845 (2 μM), MLA (125 μM), MMA (10 μM), AM-251 (2 μM), ω-CgTx (0.5 μM), and ω-Aga (250 nM).

Electrophysiology. Whole-cell voltage- and current-clamp recordings were obtained from the soma of CA1 PCs with a Cornerstone PC-ONE amplifier (DAGAN) (Fig. 1*A*), using patch pipettes (4–8 MΩ) set in place with a mechanical micromanipulator (Narishige). The pipettes used for voltage clamping were filled either with a 10 mM Cl^- internal solution (140 mM K-$MeSO_4$, 10 mM Hepes-K, and 10 mM KCl) or with a Cs^+-based solution (containing 110 mM CsCl, 30 mM K-gluconate and 10 mM Hepes-K). The Cs^+-based solution was used only in voltage-clamp conditions with the pulse protocols (see below). Both solutions also contained 0.1 mM EGTA, 4 mM Na-ATP, and 0.3 mM Na-GTP, and they were buffered to pH 7.2–7.3 with KOH. In some experiments pipettes were loaded with additional compounds in the 10-mM Cl^- pipette solution: heparin (5 mg/mL), to inhibit IP_3 receptors; BAPTA (20 mM), a fast Ca^{2+} chelator; the nonpermeable calmodulin-dependent protein kinase II peptide inhibitor 281-309 (AIP; 10 μM); the G-protein inhibitor (GDPβS; 2 mM); the protein kinase C inhibitor (chelerythrine; 2 μM); the protein kinase A inhibitor (fragment 6–22 amide; 10 μM); or the light chain of the B-type botulinum toxin (i.e., BOTOX; 0.5 μM), which inhibits SNARE protein-mediated membrane fusion of endosome complexes. Under voltage-clamp conditions the membrane was usually fixed at −75 mV, a value slightly hyperpolarized with respect to the average resting Vm (−67.9 ± 7.8 mV; $N = 248$). Neurons were accepted only when the seal resistance was >1 GΩ and the series resistance (7–14 MΩ) did not increase more than 10% during the experiment. The liquid junction potential was

measured with the 10-mM Cl^- solution (~6 mV) but not corrected. The data were low-pass filtered at 1.0 kHz or 3.0 kHz and sampled at rates between 6.0 kHz and 10.0 kHz, through a Digidata 1322A (Axon Instruments). Under current-clamp conditions the pipettes were filled with either the same 10-mM Cl^- solution (see above) or with an internal solution that contained 149 mM K-$MeSO_4$, 10 mM Hepes, 1 mM KCl, 4 mM Na-ATP, 0.3 mM Na-GTP, and 0.1 mM EGTA. The Vm was fixed to ~ −65 mV or ~ −75 mV by injecting a steady bias current as needed, and pClamp programs (Molecular Devices) were used to generate stimulus timing signals and transmembrane current pulses and to record and analyze the data. Bipolar synaptic stimulation was achieved with a pipette pulled from theta glass capillary (Ø of the tip ~20 μm), filled with ACSF, and connected through two silver-chloride electrodes to a Grass S88 stimulator and stimulus isolation unit that generated the simulation protocols by computer commands. Stimulation electrodes were placed in the SR, ~50 μm from the soma of the recorded neuron (Fig. 1*A*), and they preferentially activated perisomatic and proximal dendritic inhibition. Chemicals were purchased from Sigma-Aldrich Química, Tocris (Biogen Científica), and Alomone Laboratories.

Stimulation Protocols. Under voltage-clamp conditions, the PC was held at −75 mV and one of three depolarization protocols were used: (*i*) A TBS protocol was used that mimics the action potential discharge pattern of CA1 pyramidal neurons during the natural hippocampal theta rhythm. The PC was stimulated with brief bursts of four depolarizing voltage pulses (Fig. 1 *B* and *C*, Vm), each inducing a single action current (i.e., escape current, caused by the imperfect voltage control at the axon spike generation site) at a frequency of 30–70 s^{-1} that was repeated at 3–5 Hz. This was coupled with paired-pulse stimulation (50-ms delay) of inhibitory inputs at the SR during intervals between the action current bursts (Fig. 1 *B* and *C*, Im). (*ii*) A pulse protocol was used in which the PC was held at −75 mV and depolarized to 0 mV for 30 s every 75 s or to 5 s every 15 s, while paired-pulse (50-ms delay) stimulation of inhibitory inputs was applied at the SR every 3 s to induce IPSCs (Fig. 2 *A* and *D*). Several epochs were recorded as controls to check the stability of the response. Within 10–20 min after attaining the whole-cell configuration, a pipette loaded with ACh dissolved in distilled water (1 M) was lowered into the slice at the SR, close to the base of the apical dendritic shaft and ~50 μm from the soma of the recorded PC. Accordingly, a single 100-ms or 300-ms ACh pulse was applied iontophoretically (Fig. 1*A*), usually while the depolarization protocols were briefly interrupted (~3 min). Although ACh is taken up quickly and degraded, the ACh-loaded pipette was rapidly withdrawn to avoid the effects of spurious ACh release. This ACh pulse application procedure was designed to mimic the release of the transmitter from cholinergic septal fibers and to reduce spillover in an attempt to restrict the effects of ACh to the PC recorded. With this procedure transient inward currents (≤1 min) and increases in spontaneous IPSC/IPSP activity (≤20 s) could occur during the insertion and removal of the pipette, whereas the ACh pulse was not followed by stable increases of spontaneous IPSC activity ($P > 0.05$; $N = 248$). Hence, the effects of ACh appeared to be transient and confined to the patched PC, and they did not seem to diffuse to excite nearby inhibitory interneurons in a persistent manner (Fig. 1*F*). The effects of the ACh pulse were essentially identical when applied during interruptions in the depolarizing protocols or during the protocols, and they did not depend on the Vm or inhibitory activity (representative responses evoked in voltage- and current-clamp conditions are shown in Figs. 1*F* and 4*B*, respectively). We also stimulated the *stratum O/A* (at 50 s^{-1} during 10 s), which contains cholinergic afferents running from the septal nuclei to the hippocampus (Fig. 4*D*, *Inset*). Stimulation and recording continued for at least 30 min and usually ~1 h after the ACh pulse or *O/A* stimulation. In another series of control voltage-clamp experiments the ACh pulse was omitted but the pulse protocols and SR stimulation were maintained or the ACh pulse was applied in the absence of TBS and pulse protocols. In current-clamp experiments we used an intracellular TBS protocol consisting of four brief depolarizing current pulses, each inducing a single action potential at 30–70 s^{-1} that was coupled to paired-pulse stimulation (50-ms or 100-ms delay) of inhibitory inputs at the SR during intervals between the action potential bursts (Fig. 4*A*). This protocol was repeated at 3–5 s^{-1}. In current-clamp conditions, the ACh pulse depolarized and evoked repetitive firing of the PC (Fig. 4 *B* and *C*). No differences were observed in the membrane potential and synaptic responses in experiments performed in both sexes. The $GABA_A$-LTP was also evoked at 34–36 °C, reaching essentially identical values to those obtained at room temperature (Fig. 4 *C* and *E*–*G*). The bath temperature was controlled with an SH-27B in-line solution heater and a TC-324B controller, with the TA-29 thermistor submerged in the bath (Warren Instruments).

Data Analysis. The data were analyzed using pClamp software (Molecular Devices), and the statistical analysis was carried out using pClamp and Excel (Microsoft). IPSCs and IPSPs were averaged ($n = 10$), except when otherwise indicated. The magnitude of the change in the IPSP and IPSC peak amplitudes was expressed as the proportion (percentage) of the average basal control amplitude (of the first R1 of the pair) and plotted against time. The effects of blocking GABA release with ω-conotoxin and ω-agatoxin were tested, and the IPSC peak amplitudes were expressed as the proportion (percentage) of the steady-state amplitude reached during the $GABA_A$-LTP. Because of the constraint imposed by the 50-ms delay paired-pulse stimulation, we used a single exponential fit to describe the IPSC decay slope tau (*T*), which was calculated between 94% and 23% of the peak amplitude of the first R1 IPSC of the pair and had correlation coefficients between 0.95 and 0.99 ($P < 0.001$; $N = 25$). The plots of the relative changes in *T* values (percentage of difference from average control values) against time were constructed using values averaged over 5-min epochs. Statistical analysis was performed using a Student's two-tail *t* test and the differences were considered statistically significant at $^*P < 0.05$, $^{**}P < 0.01$, and $^{***}P < 0.001$ levels. The results are given as the mean ± SEM (N = numbers of cells).

ACKNOWLEDGMENTS. We thank Profs. Alfonso Araque, Michel Borde, and Pablo Castillo for their excellent suggestions and corrections to an earlier version of this manuscript. We also thank Prof. Vivien Chevalyre for his suggestions and for permitting S.D. to return to Madrid from his laboratory in Paris to perform the required experiments. This work was supported by Ministerio de Ciencia and Tecnología Grant BFU2005-07486 and Comunidad Autónoma de Madrid Grant GR/SAL/0877/2004 (to W.B.), and Ministerio de Ciencia e Innovación Grants BFU2008-03488 and BFU2011-23522 (to D.F.d.S.). D.F.d.S. was supported by a Ramón y Cajal Contract and is now a Professor at the Departamento de Anatomía, Histología y Neurociencia, Facultad de Medicina, Universidad Autónoma de Madrid. S.D. was a Doctoral Fellow supported by Grant BFU2005-07486 and is now a postdoctoral fellow in the team "Synaptic Plasticity and Neural Networks" at Centre National de la Recherche Scientifique, Unité Mixte de Recherche 8118, at the Université Paris Descartes.

1. Carlson G, Wang Y, Alger BE (2002) Endocannabinoids facilitate the induction of LTP in the hippocampus. *Nat Neurosci* 5(8):723–724.
2. Ormond J, Woodin MA (2011) Disinhibition-mediated LTP in the hippocampus is synapse specific. *Front Cell Neurosci* 5:17.
3. Somogyi P, Klausberger T (2005) Defined types of cortical interneurone structure space and spike timing in the hippocampus. *J Physiol* 562(Pt 1):9–26.
4. Fernández de Sevilla D, Buño W (2010) The muscarinic long-term enhancement of NMDA and AMPA receptor-mediated transmission at Schaffer collateral synapses develop through different intracellular mechanisms. *J Neurosci* 30(33): 11032–11042.
5. Fernández de Sevilla D, Núñez A, Borde M, Malinow R, Buño W (2008) Cholinergic-mediated IP3-receptor activation induces long-lasting synaptic enhancement in CA1 pyramidal neurons. *J Neurosci* 28(6):1469–1478.
6. Cea-del Rio CA, et al. (2010) M3 muscarinic acetylcholine receptor expression confers differential cholinergic modulation to neurochemically distinct hippocampal basket cell subtypes. *J Neurosci* 30(17):6011–6024.
7. McBain CJ, Kauer JA (2009) Presynaptic plasticity: Targeted control of inhibitory networks. *Curr Opin Neurobiol* 19(3):254–262.
8. Lewis PR, Shute CC (1967) The cholinergic limbic system: Projections to hippocampal formation, medial cortex, nuclei of the ascending cholinergic reticular system, and the subfornical organ and supra-optic crest. *Brain* 90(3):521–540.
9. Frazier CJ, et al. (1998) Acetylcholine activates an alpha-bungarotoxin-sensitive nicotinic current in rat hippocampal interneurons, but not pyramidal cells. *J Neurosci* 18(4):1187–1195.
10. Wanaverbecq N, Semyanov A, Pavlov I, Walker MC, Kullmann DM (2007) Cholinergic axons modulate GABAergic signaling among hippocampal interneurons via postsynaptic alpha 7 nicotinic receptors. *J Neurosci* 27(21):5683–5693.
11. Castillo PE, Chiu CQ, Carroll RC (2011) Long-term plasticity at inhibitory synapses. *Curr Opin Neurobiol* 21(2):328–338.
12. Kim J, Isokawa M, Ledent C, Alger BE (2002) Activation of muscarinic acetylcholine receptors enhances the release of endogenous cannabinoids in the hippocampus. *J Neurosci* 22(23):10182–10191.
13. Younts TJ, Chevaleyre V, Castillo PE (2013) CA1 pyramidal cell theta-burst firing triggers endocannabinoid-mediated long-term depression at both somatic and dendritic inhibitory synapses. *J Neurosci* 33(34):13743–13757.
14. Hasselmo ME (2006) The role of acetylcholine in learning and memory. *Curr Opin Neurobiol* 16(6):710–715.
15. Castillo PE, Younts TJ, Chávez AE, Hashimotodani Y (2012) Endocannabinoid signaling and synaptic function. *Neuron* 76(1):70–81.
16. Kawaguchi SY, Hirano T (2002) Signaling cascade regulating long-term potentiation of GABA(A) receptor responsiveness in cerebellar Purkinje neurons. *J Neurosci* 22(10): 3969–3976.

17. Alger BE, et al. (1996) Retrograde signalling in depolarization-induced suppression of inhibition in rat hippocampal CA1 cells. *J Physiol* 496(Pt 1):197–209.
18. Saliba RS, Gu Z, Yan Z, Moss SJ (2009) Blocking L-type voltage-gated Ca2+ channels with dihydropyridines reduces gamma-aminobutyric acid type A receptor expression and synaptic inhibition. *J Biol Chem* 284(47):32544–32550.
19. Nurse S, Lacaille JC (1999) Late maturation of GABA(B) synaptic transmission in area CA1 of the rat hippocampus. *Neuropharmacology* 38(11):1733–1742.
20. Zucker RS (1999) Calcium- and activity-dependent synaptic plasticity. *Curr Opin Neurobiol* 9(3):305–313.
21. Wang H, Wu LJ, Zhang F, Zhuo M (2008) Roles of calcium-stimulated adenylyl cyclase and calmodulin-dependent protein kinase IV in the regulation of FMRP by group I metabotropic glutamate receptors. *J Neurosci* 28(17):4385–4397.
22. McDonald BJ, et al. (1998) Adjacent phosphorylation sites on GABAA receptor beta subunits determine regulation by cAMP-dependent protein kinase. *Nat Neurosci* 1(1): 23–28.
23. Poisbeau P, Cheney MC, Browning MD, Mody I (1999) Modulation of synaptic GABAA receptor function by PKA and PKC in adult hippocampal neurons. *J Neurosci* 19(2): 674–683.
24. Malinow R, Schulman H, Tsien RW (1989) Inhibition of postsynaptic PKC or CaMKII blocks induction but not expression of LTP. *Science* 245(4920):862–866.
25. Rannals MD, Kapur J (2011) Homeostatic strengthening of inhibitory synapses is mediated by the accumulation of GABA(A) receptors. *J Neurosci* 31(48):17701–17712.
26. Bogdanov Y, et al. (2006) Synaptic GABAA receptors are directly recruited from their extrasynaptic counterparts. *EMBO J* 25(18):4381–4389.
27. Belelli D, et al. (2009) Extrasynaptic GABAA receptors: Form, pharmacology, and function. *J Neurosci* 29(41):12757–12763.
28. Vithlani M, Terunuma M, Moss SJ (2011) The dynamic modulation of GABA(A) receptor trafficking and its role in regulating the plasticity of inhibitory synapses. *Physiol Rev* 91(3):1009–1022.
29. Caraiscos VB, et al. (2004) Tonic inhibition in mouse hippocampal CA1 pyramidal neurons is mediated by alpha5 subunit-containing gamma-aminobutyric acid type A receptors. *Proc Natl Acad Sci USA* 101(10):3662–3667.
30. Pavlov I, Savtchenko LP, Kullmann DM, Semyanov A, Walker MC (2009) Outwardly rectifying tonically active GABAA receptors in pyramidal cells modulate neuronal offset, not gain. *J Neurosci* 29:15341–15350.
31. Rivera C, et al. (2004) Mechanism of activity-dependent downregulation of the neuron-specific K-Cl cotransporter KCC2. *J Neurosci* 24(19):4683–4691.
32. Woodin MA, Ganguly K, Poo MM (2003) Coincident pre- and postsynaptic activity modifies GABAergic synapses by postsynaptic changes in Cl- transporter activity. *Neuron* 39(5):807–820.
33. Acsády L, Katona I, Martínez-Guijarro FJ, Buzsáki G, Freund TF (2000) Unusual target selectivity of perisomatic inhibitory cells in the hilar region of the rat hippocampus. *J Neurosci* 20(18):6907–6919.
34. Pawelzik H, Hughes DI, Thomson AM (2002) Physiological and morphological diversity of immunocytochemically defined parvalbumin- and cholecystokinin-positive interneurones in CA1 of the adult rat hippocampus. *J Comp Neurol* 443(4):346–367.
35. Hefft S, Jonas P (2005) Asynchronous GABA release generates long-lasting inhibition at a hippocampal interneuron-principal neuron synapse. *Nat Neurosci* 8(10):1319–1328.
36. Brooks PA, Glaum SR (1995) GABAB receptors modulate a tetanus-induced sustained potentiation of monosynaptic inhibitory transmission in the rat nucleus tractus solitarii in vitro. *J Auton Nerv Syst* 54(1):16–26.
37. Capogna M, Gähwiler BH, Thompson SM (1995) Presynaptic enhancement of inhibitory synaptic transmission by protein kinases A and C in the rat hippocampus in vitro. *J Neurosci* 15(2):1249–1260.
38. Chevaleyre V, Heifets BD, Kaeser PS, Südhof TC, Castillo PE (2007) Endocannabinoid-mediated long-term plasticity requires cAMP/PKA signaling and RIM1alpha. *Neuron* 54(5):801–812.
39. Ohno-Shosaku T, et al. (2003) Postsynaptic M1 and M3 receptors are responsible for the muscarinic enhancement of retrograde endocannabinoid signalling in the hippocampus. *Eur J Neurosci* 18(1):109–116.
40. Brickley SG, Mody I (2012) Extrasynaptic GABA(A) receptors: Their function in the CNS and implications for disease. *Neuron* 73(1):23–34.
41. Nusser Z, Cull-Candy S, Farrant M (1997) Differences in synaptic GABA(A) receptor number underlie variation in GABA mini amplitude. *Neuron* 19(3):697–709.
42. Bannai H, et al. (2009) Activity-dependent tuning of inhibitory neurotransmission based on GABAAR diffusion dynamics. *Neuron* 62(5):670–682.
43. Luscher B, Fuchs T, Kilpatrick CL (2011) GABAA receptor trafficking-mediated plasticity of inhibitory synapses. *Neuron* 70(3):385–409.
44. Farrant M, Nusser Z (2005) Variations on an inhibitory theme: Phasic and tonic activation of GABA(A) receptors. *Nat Rev Neurosci* 6(3):215–229.
45. Glykys J, Mann EO, Mody I (2008) Which GABA(A) receptor subunits are necessary for tonic inhibition in the hippocampus? *J Neurosci* 28(6):1421–1426.
46. Serwanski DR, et al. (2006) Synaptic and nonsynaptic localization of GABAA receptors containing the alpha5 subunit in the rat brain. *J Comp Neurol* 499(3):458–470.
47. Ali AB, Thomson AM (2008) Synaptic alpha 5 subunit-containing GABAA receptors mediate IPSPs elicited by dendrite-preferring cells in rat neocortex. *Cereb Cortex* 18(6):1260–1271.
48. Lei S, McBain CJ (2003) GABA B receptor modulation of excitatory and inhibitory synaptic transmission onto rat CA3 hippocampal interneurons. *J Physiol* 546(Pt 2): 439–453.